Supplementary Information: Spectral kissing and its dynamical consequences in the squeezed Kerr-nonlinear oscillator

Jorge Chávez-Carlos,[1] Talía L.M. Lezama,[2] Rodrigo G. Cortiñas,[3] Jayameenakshi Venkatraman,[3] Michel H. Devoret,[3] Victor S. Batista,[4] Francisco Pérez-Bernal,[5,6] and Lea F. Santos[1]

[1]*Department of Physics, University of Connecticut, Storrs, Connecticut 06269, USA*
[2]*Department of Physics, Yeshiva University, New York, New York 10016, USA*
[3]*Department of Applied Physics and Physics, Yale University, New Haven, Connecticut 06520, USA*
[4]*Department of Chemistry, Yale University, P.O. Box 208107, New Haven, Connecticut 06520-8107, USA*
[5]*Departamento de Ciencias Integradas y Centro de Estudios Avanzados en Física, Matemáticas y Computación, Universidad de Huelva, Huelva 21071, Spain*
[6]*Instituto Carlos I de Física Teórica y Computacional, Universidad de Granada, Fuentenueva s/n, 18071 Granada, Spain*

Section I of this Supplementary Information contains details about the quantum and classical Hamiltonians of the squeezed Kerr-nonlinear oscillator and a discussion about the experimental parameters. Section II compares two plots that present the excitation energies E' as a function of the control parameter ξ, in one plot both parities are included and in the other one, only one parity sector is considered. Sections III and IV give the density of states (DOS) and the Lyapunov exponent, respectively. Section V provides additional figures for the quantum dynamics. In Sec. VI, we discuss how to derive the time interval for the initial quadratic behavior in t of the survival probability, FOTOC, and $M_2(t)$. Section VIII shows the duration of the exponential growth of the FOTOC for coherent state O.

I. QUANTUM AND CLASSICAL HAMILTONIANS

In the same way that an LC circuit is the electrical analog of a mechanical harmonic oscillator, the Josephson junction is the electrical analog of a mechanical pendulum. The Hamiltonian of a single Josephson junction is [1]

$$\hat{H} = \frac{1}{2C}\hat{Q}^2 - E_J \cos\left(\frac{2\pi}{\Phi_0}\hat{\Phi}\right),$$

where C is the circuit's capacitance, E_J is the Josephson energy, $\hat{\Phi}$ is the phase circuit variable, and $\hat{Q}$ its charge, with $[\hat{\Phi}, \hat{Q}] = i\hbar$ [1]. This is the canonical commutation relation that describes quantum circuits and is analogous to the position-momentum relation in a mechanical system. The charge enters the Hamiltonian as a quadratic kinetic energy and the circuit's phase enters via the Josephson cosine potential, and is analogous to the projection of a constant gravitational field over the vertical as in a pendulum potential [2].

One defines the bosonic operators of the circuit as a convenient calculation tool. The annihilation operator for a superconducting circuit takes the form

$$\hat{a} = \sqrt{\frac{1}{2\hbar Z}}\left(\hat{\Phi} + iZ\hat{Q}\right) \tag{S1}$$

where Z is the impedance of the circuit and $[\hat{a}, \hat{a}^\dagger] = 1$. Alternatively one can write

$$\hat{\Phi} = \Phi_{\text{zpf}}\left(\hat{a}^\dagger + \hat{a}\right), \quad \hat{Q} = iQ_{\text{zpf}}\left(\hat{a}^\dagger - \hat{a}\right), \tag{S2}$$

where $\Phi_{\text{zpf}} = \sqrt{\hbar/2\omega C} = \sqrt{\hbar Z/2}$ is the zero point spread of the phase variable, ω is the small oscillation frequency of the oscillator, and $\Phi_{\text{zpf}}Q_{\text{zpf}} = \hbar/2$. Insisting on the parallel with the mechanical oscillator, Φ_{zpf} is the electrical analog to the ground state position uncertainty and Q_{zpf} corresponds to the ground state momentum uncertainty. The capacitance C then plays the role of the particle's mass.

In the case of the SNAIL transmon used in Ref. [3], the Hamiltonian of the driven circuit, which is built by an arrangement of a few Josephson junctions, reads

$$\begin{aligned}\frac{\hat{H}(t)}{\hbar} = \omega\hat{a}^\dagger\hat{a} + \sum_{m=3}^{\infty}\frac{g_m}{m}\left(\hat{a}^\dagger + \hat{a}\right)^m \\ - i\Omega_d\left(\hat{a} - \hat{a}^\dagger\right)\cos(\omega_d t).\end{aligned} \tag{S3}$$

This is Eq. (1) in Ref. [3], where the g_n's are the circuit nonlinearities and the drive is defined by its amplitude Ω_d and its frequency ω_d, which is fixed at two times the small oscillation frequency of the oscillator to create resonant squeezing. Since nonlinearity is sourced by an arrangement of Josephson junctions in the SNAIL, the g_n coefficients are of order Φ_{zpf}^{n-2} [4]. Additionally, the magnetic flux tuning of a SNAIL permits the tunability of the oscillator's nonlinearities [5]. In particular, one can tune the values of $g_3(\Phi_B)$ and $g_4(\Phi_B)$ rather accurately. For the sake of this discussion, we will approximate the impedance of the circuit as independent from the magnetic flux.

The static effective Hamiltonian describing the system in these conditions is given by

$$\frac{\hat{H}}{\hbar} = -K\hat{a}^{\dagger 2}\hat{a}^2 + \epsilon_2(\hat{a}^{\dagger 2} + \hat{a}^2), \tag{S4}$$

where, from the microscopic theory introduced in [5], we can write the Kerr constant as $K = -\frac{3g_4}{2} + 2\frac{10g_3^2}{3\omega_d}$ and $\epsilon_2 = g_3\frac{4\Omega_d}{3\omega_d}$ [3]. This Hamiltonian is the quantum optical analog of a double-well potential [6] and the number of levels inside the wells is given by $N = \xi/\pi$ [3], where $\xi = \epsilon_2/K$ is the control parameter.

The Hamiltonian in Eq. (S4) can be factorized to read

$$\hat{H} = -K(\hat{a}^{\dagger 2} - \epsilon_2/K)(\hat{a}^2 - \epsilon_2/K).$$

This means that the coherent states $|\pm\alpha\rangle$, with $(\pm\alpha)^2 = \sqrt{\epsilon_2/K}$, are both degenerate with eigenenergy zero. Since $-\hat{H}$ is positive semidefinite, then $|+\alpha\rangle$ and $|-\alpha\rangle$ are degenerate ground states of the system and can be thought of as the ground states of the double well. Note that the bonding and antibonding superpositions $\propto (|+\alpha\rangle \pm |-\alpha\rangle)$ are exactly degenerate for all well-depths. This implies that there is no tunnel splitting between the well ground-states. This is a peculiarity of our Hamiltonian that has important consequences for the dynamics [7]. Beyond the ground state, it is only in the classical limit $\xi \to \infty$, that the degeneracy is total for the excited states. For finite values of ξ, the excited state splitting is reduced exponentially with ξ.

We note that flux tuning a SNAIL circuit allows for a Kerr-free point [8], where the Kerr constant is null. We express this condition by writing $K = \Phi_{\text{zpf}}^2\kappa(\Phi_B)$, with $\kappa(\Phi_B)$ a function crossing zero. In addition, the third-order nonlinearity responsible for the generation of squeezing remains essentially constant in the vicinity of the Kerr-free point, so we can write the scaling of the control parameter ξ as a function of the experimentally controllable variables,

$$\xi = \frac{\epsilon_2}{K} \propto \frac{\Omega_d}{\Phi_{\text{zpf}}\kappa(\Phi_B)}. \tag{S5}$$

With this expression, it is clear that the value of ξ can be increased in three different ways. One can (i) reduce the impedance of the circuit, thus reducing Φ_{zpf}, (ii) increase the microwave power of the squeezing drive Ω_d, or (iii) approach the Kerr-free point by in situ magnetic flux tuning Φ_B.

A. Classical limit

As we wrote in Methods, the experimental system admits an approximate classical description if it is initialized in a coherent state and for as long as the Hamiltonian phase space surface produces only a linear force (a quadratic Hamiltonian) over the spread of the evolving state [9]. This means that the dynamics will be generated by the Poisson bracket, since the Moyal corrections can be neglected, and no phase space interference effects will develop. This can be achieved by reducing the fluctuations of the coherent state (increasing its "mass", $\Phi_{\text{zpf}} \to 0$), or by making a comparatively large double-well system ($\Omega_d/\kappa(\Phi_B) \to \infty$). Note that reducing Φ_{zpf} comes at the price of increasing the spread in the momentum coordinate. In a Hamiltonian with quadratic kinetic energy, like Eq. (S3), this comes at a minimal cost, since no nonlinearity is experienced along the momentum (charge) axis, and the Moyal corrections remain small. Note, however, that in the presence of a Kerr nonlinearity, the Hamiltonian has a nonlinear dependence on the momentum coordinate and the classical correspondence needs to be treated carefully. This justifies taking the classical limit as a system of increasing size, $\xi \gg 1$, as in the main text, which can be achieved independently of the value of zero point fluctuations.

In the absence of dissipation, this classical Hamiltonian approximation breaks at sufficiently long times for most initial conditions. In turn, small amounts of dissipation enforce the classical dynamics [3, 10, 11]. As in [10, 12], the system discussed here is not chaotic, but since for a state initialized near the ESQPT, the evolution can be approximated by a quadratic Hamiltonian (squeezing, $\epsilon_2 \gg K$), the exponential instability is a property of both the quantum and the classical models. The evolution can be approximated as classical until the phase space distribution folds on the quartic energy wall and develops phase interferences, such as those seen in the last snapshop of the last row of the Fig. 2 in the main text [13]. This quantum-classical divergence will be regularized in a timescale set by dissipation. The possibility to experimentally explore the quantum-classical correspondence in the squeezed Kerr oscillator will be communicated elsewhere.

II. CLUSTERING OF EIGENVALUES

Figure S1 (a) is identical to Fig. 1 (b) in the main text. Figure S1 (b) is the same as Figure S1 (a), but displayed for a single parity sector with the purpose of making it evident that the clustering of the eigenvalues at $E'_{\rm ESQPT}$ happens in a single sector as well. The size $\mathcal{N}$ of the truncated Hilbert space here and everywhere in this work is chosen to guarantee the convergence of the levels analyzed.

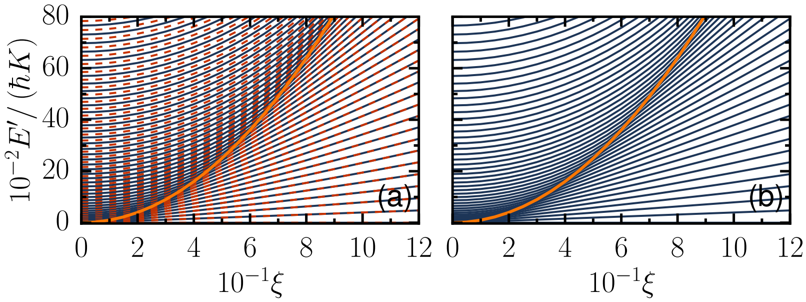

FIG. S1. Energy levels as a function of the control parameter ξ for both parity sectors (a) and for the even parity only (b). In (a): solid lines are for the energy levels in the even parity sector and dashed lines for the odd parity. The bright solid line in both panels marks the energy of the ESQPT, as given in Eq. (3) of the main text.

III. DENSITY OF STATES

We can use the lowest-order term of the Gutzwiller trace formula [15] to obtain a semiclassical approximation for the DOS,

$$\nu(\mathcal{E}) \;=\; \frac{1}{2\pi}\int dpdq\delta(H_{cl}-\mathcal{E}), \tag{S6}$$

where H_{cl} is given by

$$H_{cl} = -\frac{K_{cl}}{4}(q^2+p^2)^2 + K_{cl}\xi_{cl}(q^2-p^2), \tag{S7}$$

[Eq. (2) of the main text and with the proper sign in Eq. (11) of Methods]. To evaluate the previous integral, we use the general property of the Dirac delta,

$$\int_{\mathbb{R}^n} f(\mathbf{x})\delta(g(\mathbf{x}))d\mathbf{x} = \int_{g^{-1}(0)} \frac{f(\mathbf{x})}{|\nabla g|}d\sigma(\mathbf{x}), \tag{S8}$$

where the integral on the right is over $g^{-1}(0)$ and the $(n-1)$-dimensional surface defined by $g(\mathbf{x})=0$. Employing the property of the Dirac delta in the Gutzwiller formula, we have

$$\nu(\mathcal{E}) = \frac{1}{2\pi}\int_{q\in\Omega_{\mathcal{E}}} \frac{dq}{2\sqrt{(2\sqrt{K_{cl}\,u(\mathcal{E})}-(\lambda+K_{cl}q^2))u(\mathcal{E})}}, \tag{S9}$$

where $u(\mathcal{E}) = \mathcal{E}-\mathcal{E}_{\rm min}+\lambda q^2$, $\lambda = 2K_{cl}\xi_{cl}$, and $\Omega_{\mathcal{E}}$ is the set of values of q for which there is at least one solution of the equation $H_{cl}(q,p)=\mathcal{E}$.

IV. LYAPUNOV EXPONENT

The linear analysis around critical points gives us information about the qualitative behavior close to those points. In particular, for the Hamiltonian in Eq. (S7), the linearized Hamilton equations around a critical point $\{q_c, p_c\}$ satisfy

$$\begin{pmatrix} \dot{q} \\ \dot{p} \end{pmatrix} = \begin{pmatrix} 2K_{cl}q_c\,p_c & 2K_{cl}\xi_{cl}+K_{cl}(q_c^2+3p_c^2) \\ 2K_{cl}\xi_{cl}-K_{cl}(3q_c^2+p_c^2) & -2K_{cl}q_c\,p_c \end{pmatrix}\begin{pmatrix} q-q_c \\ p-q_c \end{pmatrix}.$$

In the equation above, *cl* stands for "classical" and *c* for "critical". The stability or instability around $\{q_c, p_c\}$ is given by the eigenvalues a_i of the matrix constructed by the linear system. If the eigenvalues of the matrix are real, then the Lyapunov exponent is equal to $\max(a_i)$. Specifically, for the critical point $\{q_c, p_c\} = \{0, 0\}$, which is a hyperbolic point, the Lyapunov exponent is given by

$$\lambda = 2K_{cl}\xi_{cl}. \tag{S10}$$

V. QUANTUM DYNAMICS

The 6 initial coherent states that we consider are those listed in Table I in Methods.

A. FOTOC

The FOTOC [16] is derived from the commutator $\langle[\hat{W}(t), \hat{V}(0)]^2\rangle$ that defines the OTOC [17–20], when the operator $\hat{V} = |\Psi(0)\rangle\langle\Psi(0)|$ is the projection operator on the initial state $|\Psi(0)\rangle$, and $\hat{W} = e^{i\delta\phi\hat{G}}$, where $\delta\phi$ is a small perturbation and $\hat{G}$ is a Hermitian operator. In the perturbative limit, $\delta\phi \ll 0$, the FOTOC is the variance $\sigma_G^2(t) = \langle\hat{G}^2(t)\rangle - \langle\hat{G}(t)\rangle^2$. In this work, we consider

$$F_{\text{otoc}}(t) = \sigma_p^2(t) + \sigma_q^2(t). \tag{S11}$$

B. Integral of the square of the Husimi function

One can quantify how an initial coherent state spreads in the phase space by computing the integral of the square of the Husimi quasiprobability distribution,

$$M_2^{\Psi(t)} = \frac{1}{2\pi}\int dq\,dp\,[Q^{\Psi(t)}(q,p)]^2, \tag{S12}$$

where $N_{\text{eff}} = 1$ and

$$Q^{\Psi(t)}(q,p) = \frac{1}{2\pi}\left|\sum_{n=0}^{\mathcal{N}} C_n(t)e^{-\frac{(q^2+p^2)}{4}}\frac{(q-ip)^n}{\sqrt{2^n n!}}\right|^2. \tag{S13}$$

By writing the evolved state in the Fock basis, $|\Psi(t)\rangle = \sum_n C_n(t)|n\rangle$, one can solve the integrals exactly and obtain

$$\begin{aligned} M_2^{\Psi(t)} =& \frac{1}{\pi}\sum_{n_1,n_2,m_1,m_2}\frac{C_{n_1}(t)C_{n_2}^*(t)C_{m_1}(t)C_{m_2}^*(t)}{\sqrt{n_1!n_2!m_1!m_2!}} \\ &\times\int d^2\alpha\, e^{-2|\alpha|^2}\alpha^{*n_1+m_1}\alpha^{n_2+m_2} \\ =& \sum_{n_1,n_2,m_1,m_2}\frac{C_{n_1}(t)C_{n_2}^*(t)C_{m_1}(t)C_{m_2}^*(t)}{\sqrt{n_1!n_2!m_1!m_2!}} \\ &\times\frac{(n_1+m_1)!}{2^{n_1+m_1+1}}\delta_{n_1+m_1,n_2+m_2}\ . \end{aligned} \tag{S14}$$

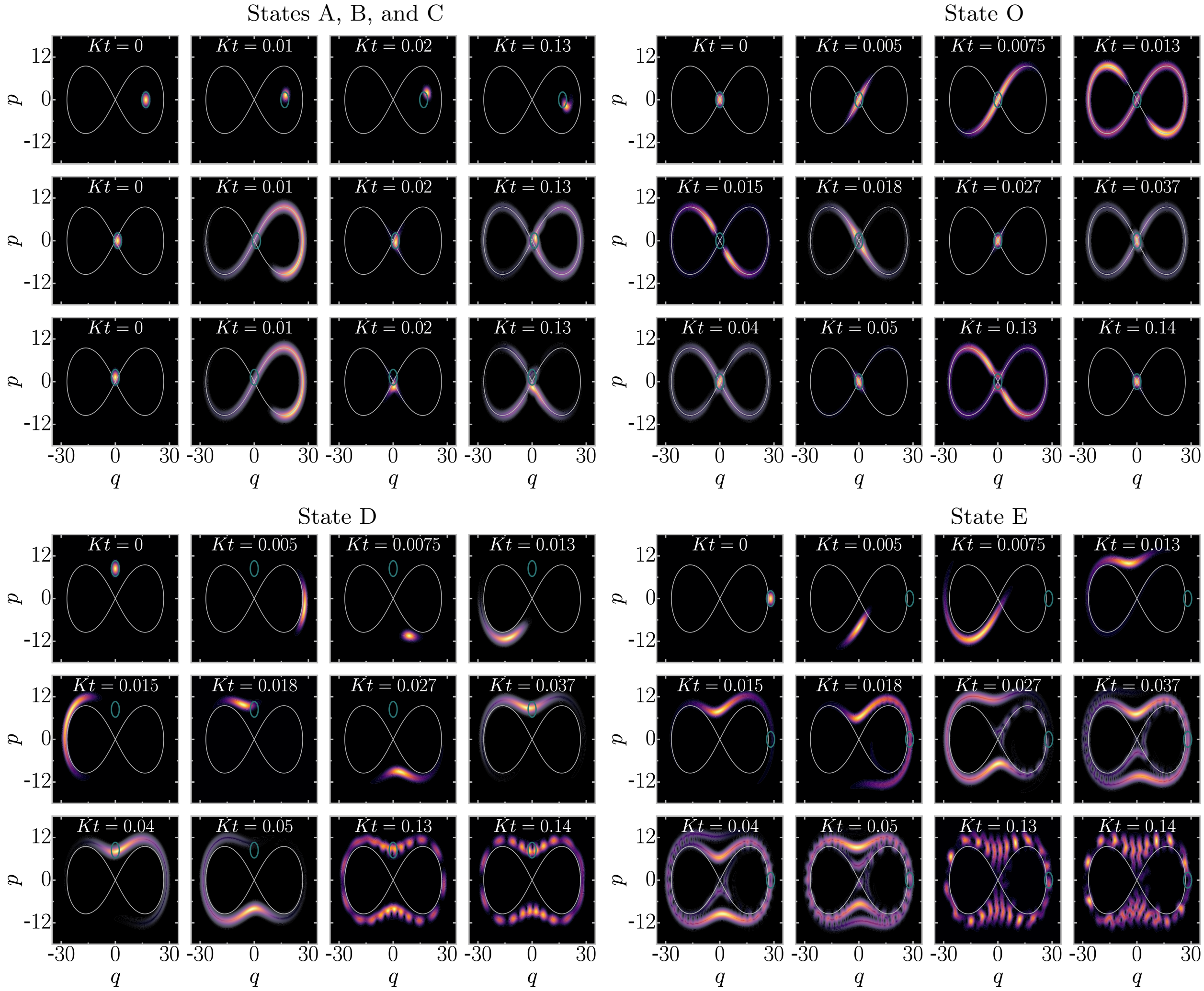

FIG. S2. Snapshots of the Husimi quasiprobability distributions for the 6 initial coherent states investigated, as indicated in the titles; $\xi = \xi_{cl} = 180$. On the top left, the snapshots in the first row of panels are for state A, in the second row they are for B, and the third row for C.

C. Snapshots of the evolution of the Husimi quasiprobability distribution

This subsection presents various snapshots of the evolution of the Husimi functions for the 6 initial coherent states investigated, including again the same cases presented in the main text for $|\Psi_O(0)\rangle$, $|\Psi_D(0)\rangle$, and $|\Psi_E(0)\rangle$. The main features are summarized below.

The three rows of panels on the top left of Fig. S2 present snapshots of the Husimi function for four instants of time for the initial coherent states $|\Psi_A(0)\rangle$ (first row), $|\Psi_B(0)\rangle$ (second row), and $|\Psi_C(0)\rangle$ (third row). State A has very low energy and thus exhibits a very limited spread around its initial region in the phase space. At $Kt = 0.02, 0.13$, the distribution gets mostly out of the green ellipse that determines the initial state, so the value of $S_p^{(A)}(t)$ should become very small.

In contrast with $|\Psi_A(t)\rangle$, the Husimi distributions for $|\Psi_B(t)\rangle$ and $|\Psi_C(t)\rangle$ get squeezed, but do not fully leave the green ellipse. These two states present evolutions similar to the coherent state $|\Psi_O(t)\rangle$, since the two also start close to the critical point at the origin of the phase space. As mentioned in the main text, the fact that $|\Psi_B(t)\rangle$ evolves towards the region with negative values of q is a quantum effect. The classical point B has a positive value of q and is inside the separatrix, so classically its orbit never reaches values of $q < 0$.

The various snapshots of the Husimi functions for $|\Psi_O(t)\rangle$ (top right), $|\Psi_D(t)\rangle$ (bottom left), and $|\Psi_E(t)\rangle$ (bottom right) complement those displayed in the main text. The panels for $|\Psi_O(t)\rangle$ make evident the fast spread of this state, and also the subsequent alternating spread and contraction of its Husimi function.

State E also spreads fast, because it is placed on the separatrix, although far from the origin. Just as for B and C, its exponential behavior is a quantum effect.

Part of the quantum evolution of the coherent state E happens inside the separatrix and part of it is outside, creating two spreading fronts, as visible from the snapshots at $Kt = 0.027, 0.037, 0.04$, and 0.05. These different paths generate a complicated pattern of interferences, as shown for $Kt = 0.13$ and 0.14. Quantum interferences also appear for the initial coherent state $|\Psi_D(0)\rangle$. This state has high energy equal to state E, but since $|\Psi_D(0)\rangle$ starts far from the separatrix, the interferences take longer to develop.

VI. QUADRATIC BEHAVIOR IN TIME

At very short times, the survival probability, FOTOC, and $M_2(t)$ present a quadratic behavior in time. The time interval for this behavior is derived by doing a Taylor expansion of the propagator $U(t) = e^{-iHt}$ as shown below.

A. Survival probability

At short times, the survival probability can be written as [21]

$$\begin{aligned} S_p(t) &= \left|\langle\Psi(0)|e^{-iHt}|\Psi(0)\rangle\right|^2 \\ &\approx \left|\left\langle\Psi(0)\left|1 - iHt - \frac{H^2t^2}{2}\right|\Psi(0)\right\rangle\right|^2 \\ &= 1 - t^2\left[\langle\Psi(0)|H^2|\Psi(0)\rangle - \langle\Psi(0)|H|\Psi(0)\rangle^2\right] \\ &= 1 - \Gamma^2 t^2, \end{aligned}$$

where Γ^2 is the variance of the energy distribution of the initial state written in the energy eigenbasis, that is

$$\Gamma^2 = \sum_k |C_k^{(0)}|^2 (E_k^2 - E_0)^2,$$

where $H|E_k\rangle = E_k|E_k\rangle$, $E_0 = \langle\Psi(0)|H|\Psi(0)\rangle$, and

$$C_k^{(0)} = \langle E_k|\Psi(0)\rangle.$$

Using the Fock basis $|n\rangle$ to write Γ_O^2 for the initial coherent state O, we have that

$$\begin{aligned} \Gamma_O^2 &= \sum_n \langle 0|H|n\rangle\langle n|H|0\rangle - \langle 0|H|0\rangle^2 \\ &= \sum_{n\neq 0} \left|\langle n|H|0\rangle\right|^2, \end{aligned}$$

therefore,

$$S_p^O(t) \approx 1 - 2\xi^2 K^2 t^2. \tag{S15}$$

This implies that the survival probability for the state O decays quadratically for

$$Kt < \frac{1}{\sqrt{2}\xi}. \tag{S16}$$

The derivation of Γ^2 for the other coherent states is analogous. As evident from Fig. 2 (d) in the main text, the state $|\Psi_O(0)\rangle$ has the smallest variance Γ_O^2, which happens because the corresponding classical point O is a stationary point. The gradient and Laplacian of the Hamitonian vanish at O, so the initial diffusion constant for the Glauber coherent state $|\Psi_O(0)\rangle$ is the smallest one.

In Fig. S3, we show the energy distributions of the coherent states O, D, and E. The width of the distribution for O is significantly narrower than for the other two states, as anticipated from the dynamics.

Another feature observed in Fig. S3 is the difference in the widths of the energy distributions for coherent states D and E. Even though both initial states have the same energy, coherent state $|\Psi_E(0)\rangle$ is more spread out than $|\Psi_D(0)\rangle$, which explains why the survival probability $S_p^E(t)$ decays faster than $S_p^D(t)$, as seen in the Fig. 2 (d) of the main text.

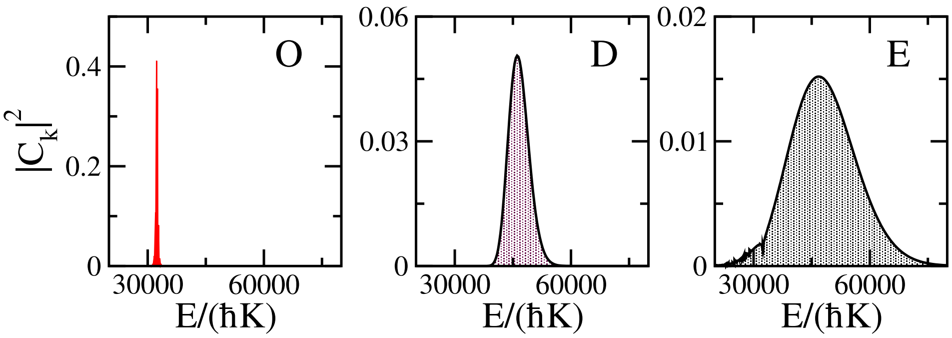

FIG. S3. Energy distribution of the coherent states O, D, and E, as indicated in the panels; $\xi = 180$, $\hbar = 1$.

B. FOTOC

The same procedure can be extended to the FOTOC, where one now needs to compute

$$\left\langle \Psi(0) \middle| \left[1 + iHt - \frac{H^2t^2}{2}\right] \hat{A} \left[1 - iHt - \frac{H^2t^2}{2}\right] \middle| \Psi(0) \right\rangle$$

up to $\mathcal{O}(t^2)$ for $\hat{A} = \hat{p}$, $\hat{A} = \hat{p}^2$, $\hat{A} = \hat{q}$, and $\hat{A} = \hat{q}^2$.

For the coherent state O, we find that

$$F_{\text{otoc}}^{(O)} \approx 1 + 8\xi^2 K^2 t^2, \tag{S17}$$

so its quadratic behavior holds for

$$Kt < \frac{1}{\sqrt{8}\xi}. \tag{S18}$$

C. Integral of the square of the Husimi function

To determine the duration of the quadratic behavior of $M_2(t)$, one needs to do the Taylor expansion for each component $C_n(t)$ in Eq. (S14), which becomes a tedious exercise even for the coherent state O. This timescale should again be dependent on the value of the control parameter, and we verify numerically that

$$Kt < \frac{1}{\xi}. \tag{S19}$$

is an upper bound.

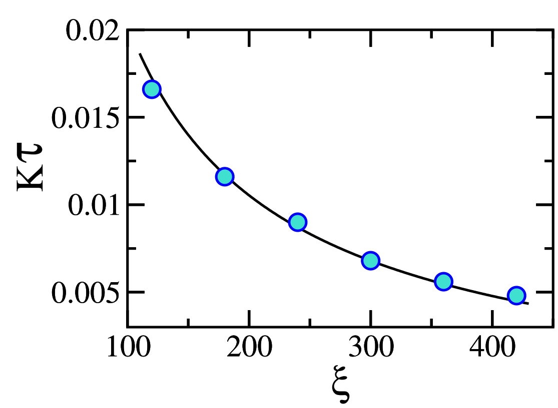

FIG. S4. Time $\mathcal{T}$ when the FOTOC for the coherent state $|\Psi_O(0)\rangle$ reaches its maximum value as a function of ξ. Symbols are for the numerical results and the solid line corresponds to the expression in Eq. (S20).

VII. EXPONENTIAL GROWTH OF THE FOTOC

The exponential growth of the FOTOC for the coherent state $|\Psi_O(0)\rangle$ holds up to the Ehrenfest time $\mathcal{T}$ [22], which in our case is given by

$$K\mathcal{T} \sim -0.0027 + \ln(\xi)/(2\xi). \tag{S20}$$

In Fig. S4, we show numerical results for $K\mathcal{T}$ as a function of ξ, and we find very good agreement with the expression in Eq. (S20).

[1] A. Blais, A. L. Grimsmo, S. M. Girvin, and A. Wallraff, Circuit quantum electrodynamics, Rev. Mod. Phys. **93**, 025005 (2021).

[2] S. M. Girvin, Circuit QED: superconducting qubits coupled to microwave photons, in *Quantum Machines: Measurement and Control of Engineered Quantum Systems: Lecture Notes of the Les Houches Summer School: Volume 96, July 2011* (Oxford University Press, 2014).

[3] N. E. Frattini, R. G. Cortiñas, J. Venkatraman, X. Xiao, Q. Su, C. U. Lei, B. J. Chapman, V. R. Joshi, S. M. Girvin, R. J. Schoelkopf, S. Puri, and M. H. Devoret, The squeezed Kerr oscillator: spectral kissing and phase-flip robustness (2022), arXiv:2209.03934.

[4] J. Venkatraman, X. Xiao, R. G. Cortiñas, A. Eickbusch, and M. H. Devoret, Static effective Hamiltonian of a rapidly driven nonlinear system, Phys. Rev. Lett. **129**, 100601 (2022).

[5] N. E. Frattini, U. Vool, S. Shankar, A. Narla, K. M. Sliwa, and M. H. Devoret, 3-wave mixing Josephson dipole element, Appl. Phys. Lett. **110**, 222603 (2017).

[6] B. Wielinga and G. J. Milburn, Quantum tunneling in a Kerr medium with parametric pumping, Phys. Rev. A **48**, 2494 (1993).

[7] J. Venkatraman, R. G. Cortinas, N. E. Frattini, X. Xiao, and M. H. Devoret, Quantum interference of tunneling paths under a double-well barrier (2022), arXiv:2211.04605.

[8] V. Sivak, N. Frattini, V. Joshi, A. Lingenfelter, S. Shankar, and M. Devoret, Kerr-free three-wave mixing in superconducting quantum circuits, Phys. Rev. Applied **11**, 054060 (2019).

[9] T. L. Curtright, D. B. Fairlie, and C. K. Zachos, *A concise treatise on quantum mechanics in phase space* (World Scientific Publishing Company, 2013).

[10] W. H. Zurek and J. P. Paz, Decoherence, chaos, and the second law, Phys. Rev. Lett. **72**, 2508 (1994).

[11] S. Habib, K. Shizume, and W. H. Zurek, Decoherence, chaos, and the correspondence principle, Phys. Rev. Lett. **80**, 4361 (1998).

[12] W. H. Zurek and J. P. Paz, Zurek and Paz reply:, Phys. Rev. Lett. **75**, 351 (1995).

[13] W. H. Zurek, Decoherence and the transition from quantum to classical – revisited (2003), arXiv:quant-ph/0306072.

[14] A. Sugita and H. Aiba, Second moment of the Husimi distribution as a measure of complexity of quantum states, Phys. Rev. E **65**, 036205 (2002).

[15] M. C. Gutzwiller, *Chaos in Classical and Quantum Mechanics* (Springer, New York, 1990).

[16] R. J. Lewis-Swan, A. Safavi-Naini, J. J. Bollinger, and A. M. Rey, Unifying scrambling, thermalization and entanglement through measurement of fidelity out-of-time-order correlators in the Dicke model, Nat. Comm. **10**, 1581 (2019).

[17] A. Kitaev, KITP talk.

[18] J. Maldacena and D. Stanford, Remarks on the Sachdev-Ye-Kitaev model, Phys. Rev. D **94**, 106002 (2016).

[19] E. B. Rozenbaum, S. Ganeshan, and V. Galitski, Lyapunov exponent and out-of-time-ordered correlator's growth rate in a chaotic system, Phys. Rev. Lett. **118**, 086801 (2017).

[20] J. Chávez-Carlos, B. López-del Carpio, M. A. Bastarrachea-Magnani, P. Stránský, S. Lerma-Hernández, L. F. Santos, and J. G. Hirsch, Quantum and classical Lyapunov exponents in atom-field interaction systems, Phys. Rev. Lett. **122**, 024101 (2019).

[21] M. Távora, E. J. Torres-Herrera, and L. F. Santos, Power-law decay exponents: A dynamical criterion for predicting thermalization, Phys. Rev. A **95**, 013604 (2017).

[22] D. Shepelyansky, Ehrenfest time and chaos, Scholarpedia **15**, 55031 (2020).